

# A study on the evolution of subsurface deformation in a Zr-based bulk metallic glass during spherical indentation

Byung-Gil Yoo and Jae-il Jang<sup>1</sup>

Division of Materials Science and Engineering, Hanyang University, Seoul 133-791, Korea

E-mail: [jjang@hanyang.ac.kr](mailto:jjang@hanyang.ac.kr)

Received 6 August 2007, in final form 7 September 2007

Published 12 March 2008

Online at [stacks.iop.org/JPhysD/41/074017](http://stacks.iop.org/JPhysD/41/074017)

## Abstract

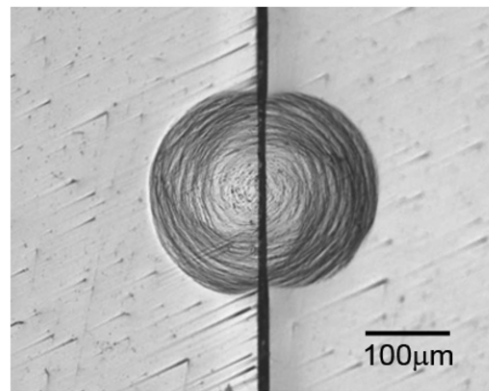
Due to its several advantages, including a simple testing procedure and the use of a small volume of material, the instrumented indentation technique has been widely performed to elucidate the characteristics of plasticity in bulk metallic glasses (BMGs) which typically show very different deformation behaviour from that of crystalline counterparts. As an effort to shed additional light on the topics, here we examined the inhomogeneous plastic deformation of a Zr–Cu–Ni–Al–Ti BMG by performing both macroscopic instrumented indentation (with a spherical indenter) and nanoindentation (with a three-sided pyramidal Berkovich indenter) on the interface-bonded sample as well as on a bulk sample. Especially, we put emphasis on analysing the evolution of shear-band-ruled deformation generated underneath the indenter during spherical indentation. It was revealed that the inter-band spacing and the shear band density are independent of indentation load and thus stress level. Furthermore, subsequent performance of nanoindentation showed that the subsurface region under the indenter was indeed softened and had quite different deformation characteristics from that of the un-deformed region.

## 1. Introduction

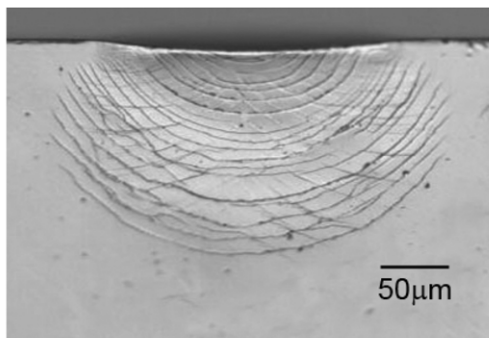
Bulk metallic glasses (BMGs) are known to show a unique plastic deformation at low temperature and high stress, i.e. once plasticity is initiated, it is highly localized into very narrow zones (so-called shear bands). As a result, the stress–strain curve from uni-axial tensile or compressive test of a BMG specimen generally exhibits very limited plastic strain (typically, less than 2%) [1, 2]. Recently, instrumented indentation techniques across multi-scale from macro- to nano-level have been widely used for analysing this interesting phenomenon of BMGs. Despite the complex nature of stress and strain under the indenter, there are many advantages in applying a instrumented indentation technique (especially nanoindentation) to this research field; for example, (1) it can provide the load–displacement ( $P$ – $h$ ) curve during the entire loading/unloading sequence, and (2) needs only a small volume of the testing material [3, 4]. In particular, a new focus of many indentation works on BMGs is their inhomogeneous

plastic flow during indentation experiments [5]. A number of studies have reported reproducible ‘serrations’ (serial pop-ins) in the nanoindentation  $P$ – $h$  curve and now it is well accepted that the serrations are associated with shear bands nucleation and/or propagation [6–10]. Nevertheless, there have been difficulties in assessing practical shear banding phenomena during indentation, simply because the shear bands are often captured beneath the indenter and cannot expand to a free surface [11]. To overcome these difficulties, very recently Ramamurty *et al* [12–15] have extensively applied the ‘interface-bonding technique’ to explore the subsurface deformation of BMGs underneath the indenter, and some other researchers have also adopted the technique for similar purposes [16, 17]. Although the interface-bonded samples cannot generate exactly the same fields of stress and strain under the indenter as those in a bulk sample without interface, one might gain insights for better understanding the governing deformation mechanism during indentation by observing the subsurface deformation morphology of the samples [12]. However, it is notable that previous studies have been mostly

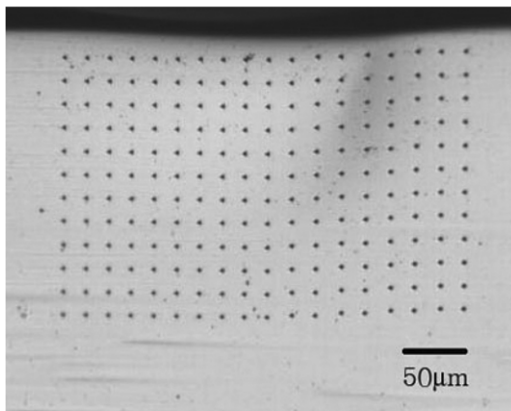
<sup>1</sup> Author to whom any correspondence should be addressed.



(a)



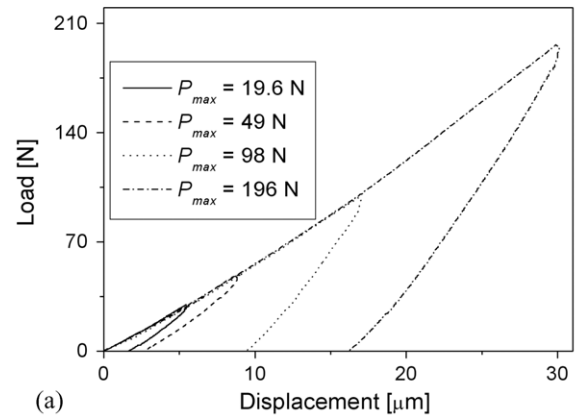
(b)



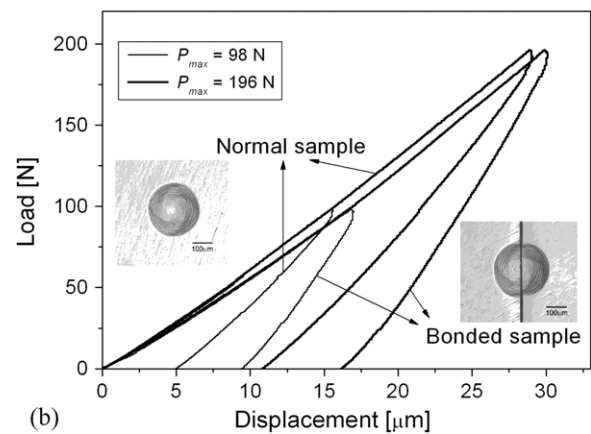
(c)

**Figure 1.** Optical micrographs demonstrating the testing procedure applied in this work: (a) macroscopic indentation on the bonded interface with a spherical indenter; (b) observation of subsurface deformation morphology and (c) nanoindentation after gentle polishing of the deformed region.

limited to the analysis of the subsurface deformation induced by Vickers indentation at different loads [12–14,16, 17] or by spherical indentation at a specific given load [15]. Unlike indentation with a geometrically self-similar sharp indenter (such as the Berkovich indenter and Vickers indenter), indentation with a spherical indenter produces an increase in ‘representative’ strain as the applied load is increased. It is well accepted that the representative strain is proportional to  $a/R = \sin \beta$  ( $= \tan \beta$  if deformation is small) where  $a$  is the contact radius,  $R$  is the indenter radius and  $\beta$  is the inclination of the indenter face to the sample surface [18]. Therefore, by



(a)



(b)

**Figure 2.** Typical load-displacement ( $P$ - $h$ ) curves obtained from macro-scale spherical indentations: (a) indentation on the bonded interface at various maximum loads from 19.6 to 196 N and (b) comparison of  $P$ - $h$  curves from a bonded-interface sample and a normal bulk sample.

analysing the subsurface morphology of spherical indentation made at various loads, somewhat new insights into the inhomogeneous plastic deformation of BMGs might be gained.

With this in mind, here we examined the inhomogeneous plastic flow of a Zr–Cu–Ni–Al–Ti BMG during indentation by performing both macroscopic instrumented indentation (with a spherical indenter) and nanoindentation (with a three-sided pyramidal Berkovich indenter) on interface-bonded samples as well as bulk samples. Especially, we put emphasis on elucidating the evolution of shear-band-ruled deformation underneath the indenter with increase in the maximum load of spherical indentation.

## 2. Experimental

Material examined in this work is a Zr-based BMG,  $Zr_{52.5}Cu_{17.9}Ni_{14.6}Al_{10}Ti_5$ , which was obtained in a rod type sample. Specimens for the interface-bonding technique were prepared by cutting the rod first into two halves and then polishing them to a mirror finish prior to bonding them using a high-strength adhesive. Following this, the top surface of the bonded specimen was polished so that it was flat like a mirror. On the bonded interface, macro-scale indentations were carried out using instrumented indentation equipment, AIS-2100 (Frontics Inc., Seoul, Korea), with a WC spherical indenter

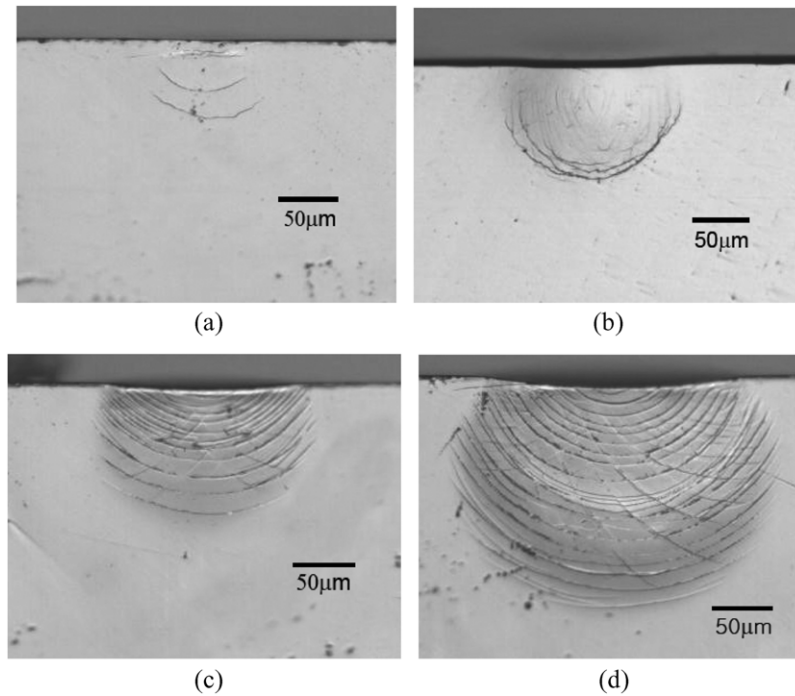


**Figure 3.** Representative examples of optical micrographs showing the development of the subsurface deformation underneath the indentation made at various peak loads:  $P_{\max} = (a)$  19.6,  $(b)$  49,  $(c)$  98 and  $(d)$  196 N.

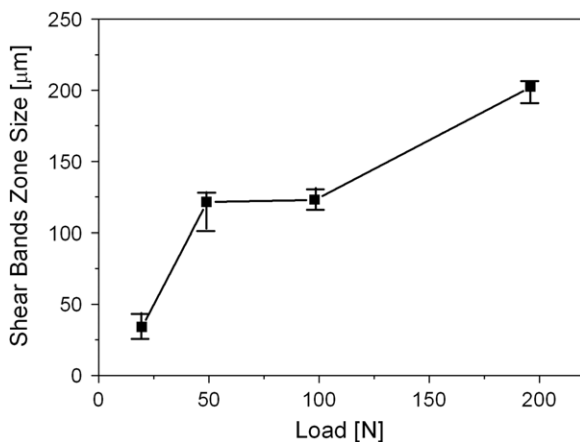


**Figure 4.** Variation in shear bands zone size as a function of indentation peak load.

having a radius of  $500 \mu\text{m}$  (see figure 1(a)). The maximum indentation loads were varied from 19.6 to 196 N, and loading rate was fixed as  $5 \mu\text{m s}^{-1}$ . After spherical indentation, the bonded interface was opened by dissolving the adhesive in acetone, and then the subsurface deformation morphology was observed through optical microscopy (figure 1(b)).

Subsequently, the subsurface deformation zone was polished again into a flat surface using alumina particles of  $0.3 \mu\text{m}$  or diamond paste of  $0.5 \mu\text{m}$ . In order to evaluate the hardness distribution within the subsurface deformation region, a series of nanoindentation experiments were performed on the gently polished surface using a Nanoindenter-XP (MTS Corp., Oak Ridge, TN) with a commonly used Berkovich indenter having centreline-to-face angle of  $65.3^\circ$  (figure 1(c)). The maximum indentation load

and the loading rate were  $50 \text{ mN}$  and  $0.5 \text{ s}^{-1}$ , respectively. To avoid possible artefacts, thermal drift was maintained below  $0.05 \text{ nm s}^{-1}$ , and more than five indentation tests under each testing condition were performed on the sample. After nanoindentation testing, the profiles of the indented surfaces were examined by atomic force microscopy (AFM) XE-100 (PSIA, Suwon, Korea).

### 3. Results and discussion

Figure 2(a) shows representative load–displacement ( $P$ – $h$ ) curves observed during macroscopic spherical indentation on the bonded-interface samples at different loads from 19.6 to 196 N. Since the effect of the soft adhesive on the overall deformation increases with decreasing indentation load, indentations at  $P_{\max} = 19.6$  and 49 N exhibited a little larger scatter in  $P$ – $h$  curves than those at  $P_{\max} = 98$  and 196 N. The influence of the soft adhesive is clearly seen in figure 2(b) which demonstrates both  $P$ – $h$  curves from a bonded-interface sample and a normal bulk sample without interface. As mentioned earlier, despite the difference in mechanical responses from the bonded-interface sample (under plane-stress condition) and the normal bulk sample (under plane-strain condition), it is generally believed that observation of the subsurface deformation morphology provides some useful clue to better understand the governing deformation mechanism [12–17]. One might imagine that the soft adhesive effect can be avoided if the mechanical clamping method is applied for bonding the interface instead of using adhesive, as in some previous studies [14, 19]. However, it should be noted that clamping the sample in a vice can induce a large additional stress in the specimen, which conceivably results in

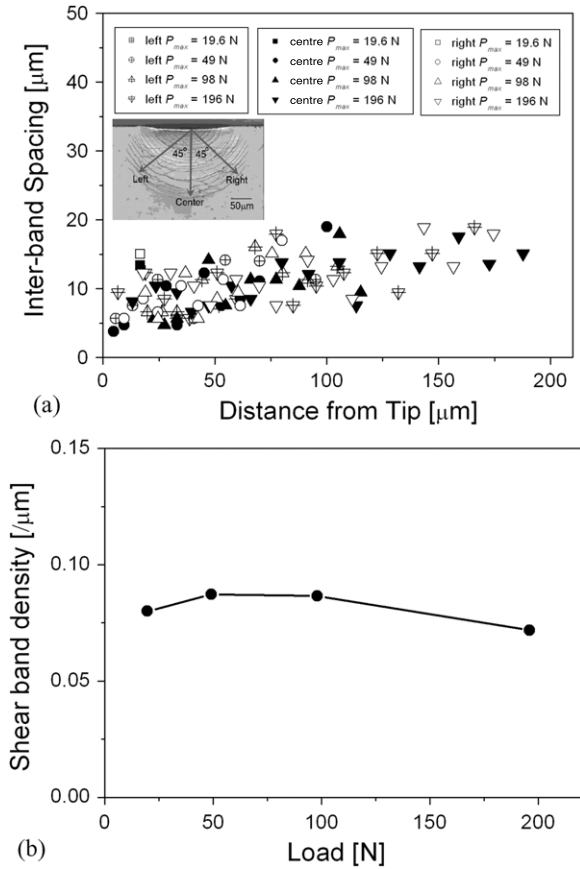
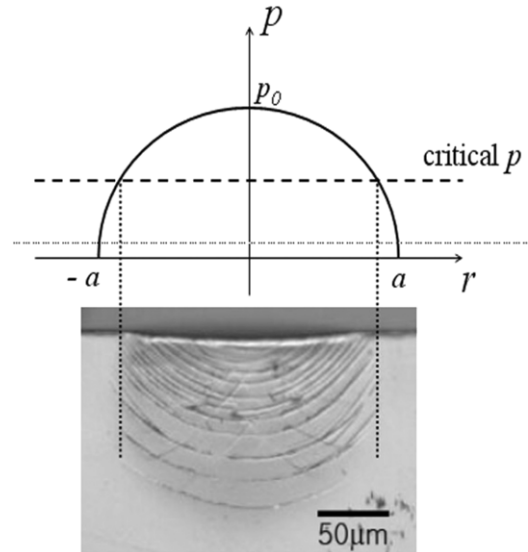


**Figure 5.** Change in subsurface deformation morphology: (a) change in inter-band spacing with indentation load and distance from indenter tip (inset shows the measurement direction) and (b) change in shear band density (measured along the centre direction, shown in (a)) with indentation load.

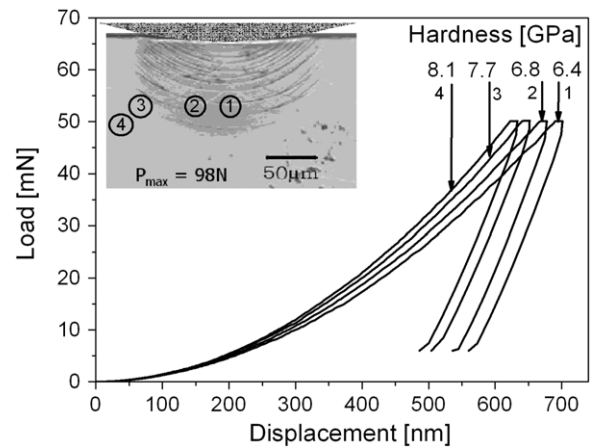
a significant constraint of the plasticity in the material during indentation.

Figure 3 gives optical micrographs showing the deformation regions underneath the hardness impressions produced at different loads. It is clearly seen that the deformed zone having multiple shear bands is evolutionally increasing as the maximum load of spherical indentation increases. The observed shear bands can be categorized into two types; semi-circular and radial shear bands. For the indentation at 19.6 N (figure 3(a)), only a few semi-circular shear bands were observed and a shear-bands-free region exists between the first shear bands and the free surface. At 49 N (figure 3(b)), the deformed zone increases in size and a few secondary, radial shear bands begin to appear. The tendency for the increase in deformed zone size with increasing load continues at higher loads such as 98 N and 196 N (figures 3(c) and (d)). At such high loads, the deformed region is almost fully filled with a large number of shear bands, and evolution of both semi-circular and radial shear bands is clearly seen.

Quantitative measurement of shear bands zone size was carried out for more than five bonded-interface specimens (i.e. more than ten surfaces which were bonded), and the results are shown in figure 4. While the shear bands zone continuously developed with increasing load as expected, interestingly, there is almost no change in its size between 49 and 96 N. Although



**Figure 6.** Schematic illustration of local pressure distribution for elastic contact according to Hertzian contact theory.



**Figure 7.** Representative  $P-h$  curve recorded during nanoindentation on different regions underneath the macroscopic indentation impression.

this abnormal phenomenon has not been well understood, it might arise from the larger influence of the soft adhesive in low load indentations (at 19.6 and 49 N) than in high load indentations (at 98 and 196 N). A relatively large scatter in the size measured from low load indentations (see figure 4) supports this postulate.

Figure 5(a) exhibits the variation in the spacing of semi-circular shear bands as functions of both indentation load and the distance from the indenter tip along the three different directions. The measured inter-band spacing was in the range 5–20  $\mu\text{m}$ , which is similar to the values for a Zr–Cu–Ti–Ni–Be BMG previously reported [15]. In spite of the fluctuation in the value, the inter-band spacing is almost independent of the load and the distance from the tip. Consistently, line density of the shear bands measured along the centre line in figure 5(b) demonstrates only a slight decrease with indentation load (see figure 5(b)). This independence of inter-band spacing might imply that the nature of shear band nucleation/propagation does not significantly change with the stress level if the stress

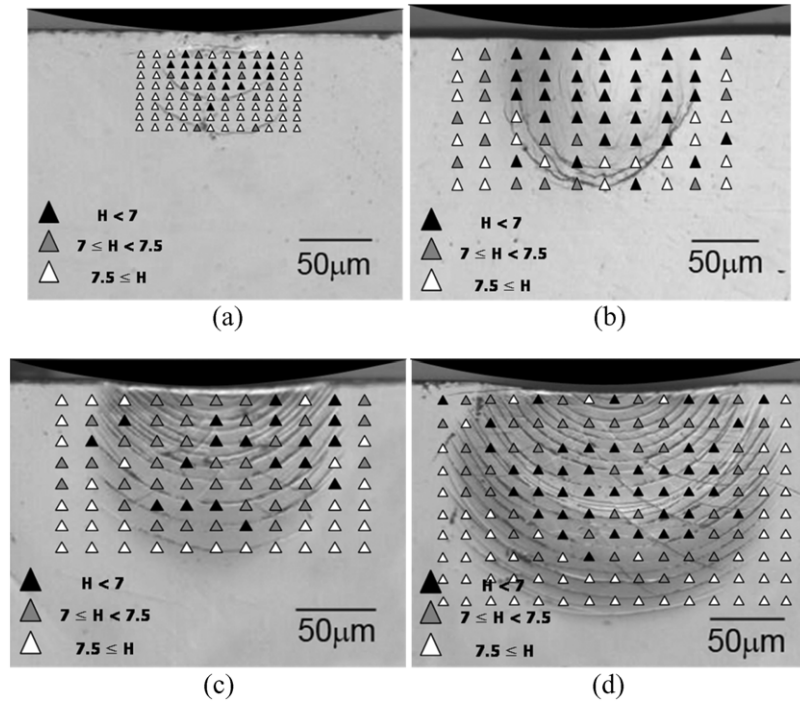


**Figure 8.** Hardness distribution underneath the indentation made at various peak loads:  $P_{\max} = (a) 19.6, (b) 49, (c) 98$  and  $(d) 196$  N.

exceeds the critical value, as argued by Ramamurty *et al* [14]. This is associated with the characteristics of the materials exhibiting elastic–perfectly plastic deformation behaviour. In such materials, the extent of additional plastic deformation is independent of stress level once the stress level is higher than the critical value, i.e. yield strength.

On the other hand, it is interesting to find that the end of each semi-circular shear band did not reach the free surface (see figure 3). One might explain this in simple consideration of Hertzian pressure distribution [18] schematically shown in figure 6, though a more accurate analysis of the stress distribution can be achieved by finite element simulation based on Mohr–Coulomb or Drucker–Prager yield criteria [2]. According to classic Hertzian contact theory [18], local pressure distribution under the spherical indenter during elastic contact can be simply described as

$$p(r) = p_0 \sqrt{1 - \frac{r^2}{a^2}}, \quad 0 \leq r \leq a, \quad (1)$$

where  $p_0$  is peak pressure,  $a$  is the ‘elastic’ contact radius and  $r$  is the radial coordinate in the surface, as shown in figure 6. If we consider that the yielding of BMGs (known to show approximately elastic–perfectly plastic deformation without work hardening) occurs when local pressure is higher than critical pressure value, the local pressure of the shear-band-free region is conceivably lower than the critical value.

Next, in order to analyse the mechanical response of the deformed region, nanoindentation experiments were performed. Figure 7 shows a typical example of  $P$ – $h$  curves recorded during indentations on different subsurface regions. There is a clear difference in  $P$ – $h$  curve and thus the hardness value; hardness values of the extensively deformed regions (regions 1 and 2 in the figure) are significantly lower than those

of the region near shear bands (region 3) and un-deformed region (region 4). Note that we could not intentionally make a nanoindentation between the shear bands or inside a shear band, simply because the shear band zone was gently polished before nanoindentation. Thus, the fluctuation of the hardness even in the extremely deformed region might arise from the uncertainty of the location where nanoindentation was made (i.e. between the shear bands or inside a band). It is also notable that the nanoindentation hardness values were calculated according to the Oliver–Pharr method so that they are overestimated rather than the real value, as the Oliver–Pharr method cannot take into consideration the pile-up typically observed around the hardness impression of BMGs [20].

Nanoindentation hardness distribution within the region underneath indentation impression is mapped in figure 8 with a background of optical microscopy image for the subsurface deformation morphology. It was found that the shear bands zones were indeed softened although there was some fluctuation in the hardness value. As shown in figure 9, as indentation load increases, the tendency for the change in the softened zone size (i.e. black triangle points in figure 8, whose hardness is lower than 7 GPa) is in good agreement with that for the variation in the shear bands zone size. The nanoindentation hardness value for the softened zone is plotted in figure 10 as a function of indentation load. High load indentations show slightly lower hardness values than low load indentation, which implies that the extent of softening keeps increasing as spherical indentation load is increasing. Very recently Bei *et al* [21] reported in their paper on the same BMG as used here that the hardness of the compressed sample was decreasing as compressive plastic strain increases. Since representative plastic strain for a spherical indentation increases with the indentation load, the tendency for hardness

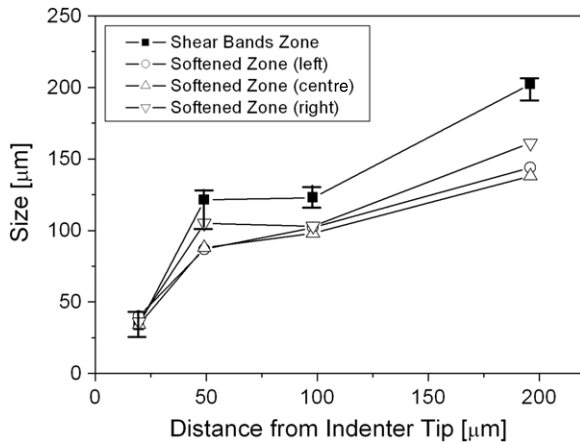


**Figure 9.** Comparison of shear band zone size and softened zone size underneath the indentation.

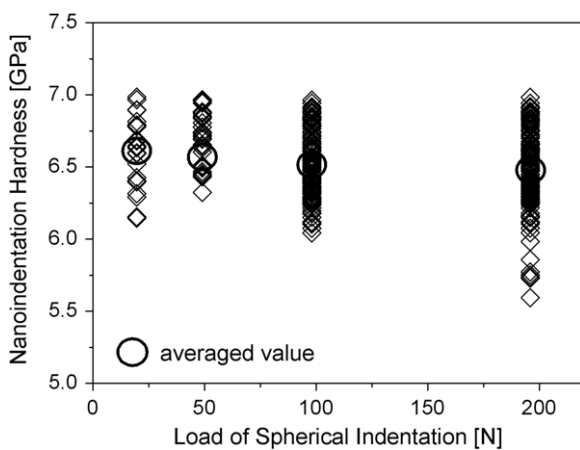


**Figure 10.** Variation in nanoindentation hardness with increase in the load of spherical indentation.

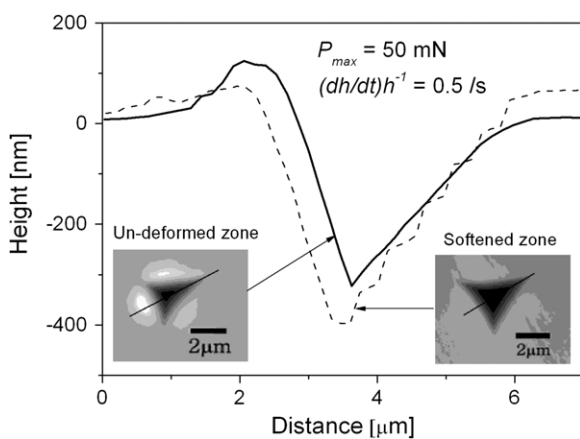


**Figure 11.** Typical example of AFM analysis of the hardness impressions made in softened region and in un-deformed region.

versus indentation load observed here is well matched with Bei *et al*'s [21] results.

Deformation behaviour of softened and normal (un-deformed) regions was examined in more detail using AFM. A representative example of the AFM work is shown in figure 11. The AFM image taken from the hardness impression of the

un-deformed region shows higher height contrast around the indentation, which is due to the material pile-up, than that of the softened region. In the line scan profile across the hardness impression, it is clearly seen that (1) the final indentation displacement for the softened region is higher than that for the normal (un-deformed) region, and (2) the pile-up in the normal region is more significant than that in the softened region. Tang *et al* [22], who made nanoindentation on the free surface around spherical indentation impression, reported a similar pile-up observation to that in this work, i.e. the smaller pile-up in the deformed region around the impression. However, in contrast, the softened region exhibited bigger pile-up than the un-deformed region in a recent work by Bhowmick *et al* [15] who performed both spherical indentation and nanoindentation on a bonded-interface sample as was done in this work.

Severe material pile-up around indentation is the nature of a material without work (strain) hardening behaviour; i.e. due to the incompressibility of the material, the material removed from the indented volume can pile-up around the indentation. According to the free volume model by Spaepen [23], a considerable amount of excess free volume can be produced in the plastic zone under the indenter during the macroscopic spherical indentation. During subsequent nanoindentation, the produced excess free volume can enhance the ability to accommodate plastic deformation induced by nanoindentation. This might result in a smaller pile-up in the deformed region than in the un-deformed region.

#### 4. Conclusion

In this paper, we have reported our recent observation on the evolution of subsurface plastic deformation in a Zr-based BMG during spherical indentation. It was revealed that the interband spacing and the shear band density are independent of indentation load and thus stress level. Furthermore, additional nanoindentation experiments showed that the subsurface region under the indenter was indeed softened and had quite different deformation characteristics from that of the un-deformed region. To better understand the subsurface deformation generated during spherical indentation, extensive comparisons of the finite element simulation results for the spherical indentation (based on the Mohr–Coulomb or the Drucker–Prager criteria) and experimental results found here are desirable.

#### Acknowledgments

This research was supported by the Korea Research Foundation Grant funded by the Korean Government, MOEHRD (Grant No KRF-2006-331-D00273). The authors would like to thank Dr H Bei (at Oak Ridge National Laboratory) for providing the valuable sample.

#### References

[1] Wang W H, Dong C and Shek C H 2004 *Mater. Sci. Eng. R* **44** 45

- [2] Schuh C A, Hufnagel T C and Ramamurty U 2007 *Acta Mater.* **55** 4067
- [3] Oliver W C and Pharr G M 1992 *J. Mater. Res.* **7** 1564
- [4] Oliver W C and Pharr G M 2004 *J. Mater. Res.* **19** 3
- [5] Schuh C A and Nieh T G 2004 *J. Mater. Res.* **19** 46
- [6] Schuh C A and Nieh T G 2003 *Acta Mater.* **51** 87
- [7] Schuh C A, Lund A C and Nieh T G 2004 *Acta Mater.* **52** 5879
- [8] Greer A L, Castellero A, Madge S V, Walker I T and Wilde J R 2004 *Mater. Sci. Eng. A* **375–377** 1182
- [9] Wei B C, Zhang L C, Zhang T H, Xing D M, Das J and Eckert J 2007 *J. Mater. Res.* **22** 258
- [10] Jang J-I, Yoo B-G and Kim J-Y 2007 *Appl. Phys. Lett.* **90** 211906
- [11] Yoo B-G, Kim J-Y and Jang J-I 2007 *Mater. Trans.* **48** 1765
- [12] Jana S, Ramamurty U, Chattopadhyay K and Kawamura Y 2004 *Mater. Sci. Eng. A* **375–377** 1191
- [13] Jana S, Bhowmick R, Kawamura Y, Chattopadhyay K and Ramamurty U 2004 *Intermetallics* **12** 1097
- [14] Ramamurty U, Jana S, Kawamura Y and Chattopadhyay K 2005 *Acta Mater.* **53** 705
- [15] Bhowmick R, Raghavan R, Chattopadhyay K, Ramamurty U 2006 *Acta Mater.* **54** 4221
- [16] Zhang H, Jing X, Subhash G, Kecskes L J and Dowding R J 2005 *Acta Mater.* **53** 3849
- [17] Li W H, Zhang T H, Xing D M, Wei B C, Wang Y R and Dong Y D 2006 *J. Mater. Res.* **21** 75
- [18] Johnson K L 1987 *Contact Mechanics* (Cambridge: Cambridge University Press)
- [19] Shan G B, Li J X, Yang Y Z, Qiao L J and Chu W Y 2007 *Mater. Lett.* **61** 1625
- [20] Wright W J, Saha R and Nix W D 2001 *Mater. Trans. JIM* **42** 642
- [21] Bei H, Xie S and George E P 2006 *Phys. Rev. Lett.* **96** 105503
- [22] Tang C, Li Y and Zeng K 2004 *Mater. Sci. Eng. A* **384** 215
- [23] Spaepen F 1977 *Acta Metall.* **25** 407